Surface modified mesoporous g-C_3N_4@FeNi_3 as prompt and proficient magnetic adsorbent for crude oil recovery

Meenakshi Talukdar, Sushant Kumar Behera, Kakoli Bhattacharya and Pritam Deb*

Advanced Functional Material Laboratory, Department of Physics,
Tezpur University (Central University), Tezpur-784028, India.

(Dated: December 20, 2018)

Efficient oil adsorption and recovery is a generous universal importance for future energy demand and environmental protection. Adsorbents based on 2D flatland with engineered surfaces can overcome the limitations of conventional methods for selective oil absorption. Here, we report magnetic hydrophobic/oleophilic graphitic C_3N_4 nanosheets that exhibit excellent oil sorption performance and ready removal of adsorbed oil using magnetic field. Combining porous and nanosheet structure along with magnetic FeNi_3 and fatty acid surface functionalization make the system an ideal adsorbent for adsorbing and separating viscous crude oil from water. The nanocomposite can be further recycled and reused in an ecofriendly manner for oil adsorption and recovery. The graphitic sheets selectively absorb a wide range of drilled oils with enhancement of thickness upto 9 folds than the pristine one. Oil can be collected and recovered with high efficiencies once, it gets adsorbed by the adsorbent.

keywords: graphitic carbon nitride . hydrophobicity and oleophilicity . magnetic nanocomposite . oil-water sorbent . oil separation.

Crude oil is important and predominant energy resource in present human societies. The availability of crude oil needs to be increased to match the rapidly growing consumption. Hence, the proficient recovery of spilled oil from oily-water is an importance concern. During crude oil exploration, a vast amount of oil in mud is generated and wasted causing soil pollution [1]. The wastage of oil during drilling not only leads to compromisation on future fuel consumption, but also creates significant threats to environment and human health. On the other side, oil spills often causes immediate and long term environmental damage [2]. The oil spillage can be cleaned traditionally by mechanical collection [3], absorbent materials [4], chemical dispersants [5], bioremediations [6], in situ burning [7], dispersants [8], solidifiers [9], skimmers [10], etc. These conventional oil-removal technologies fail to meet the required efficiency without affecting the ecosystem. In order to sustain the crude oil sources for future generations, it is required to adopt corrective means for maximum utilization and minimum wastage.

While developing an effective treatment method, it is essential to choose an appropriate adsorbing material to yield oil from water surface. Worldwide efforts are underway for developing sorption material with optimum water repelling property (i.e. hydrophobicity) as well as oil adsorption capacity (i.e. oleophilicity) for practical utilization. Oil adsorption generally follows three primary steps, like the diffusion of oil molecules into the sorbent surface, capillary entrapment of the same molecules in the sorbent structure and oil droplet agglomeration in the porous structure of the sorbent
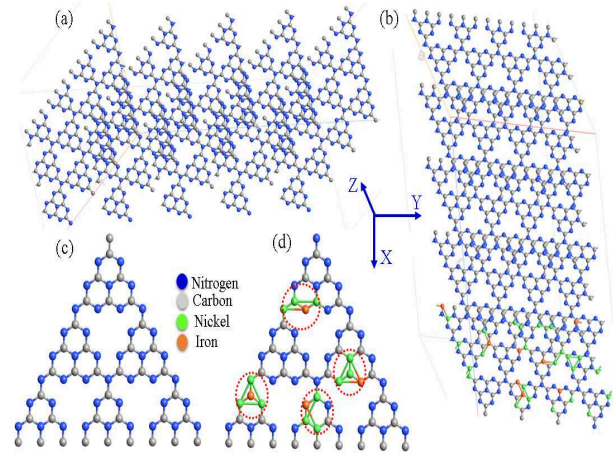

FIG. 1. Surface atomic configuration of (a) g-C_3N_4 layer structure with a interplanner spacing of 12 $\mathring{A}$, (b) composite of g-C_3N_4 and FeNi_3 where the FeNi_3 is stabilized on surface of the layer structure, monolayers of (c) g-C_3N_4 and (d) composite. Color codes of the respective atoms are marked in the figure. Dotted red circle shows the presence of FeNi_3 on g-C_3N_4 surface.

[11]. In this regard, few of the synthetic and natural sorption materials, with both hydrophobic and oleophilic properties, have been investigated and tested for oil-removal purpose [12]. An active area of research in this regard is to optimize adsorption performance, where the surface area plays major role [13]. Primarily, they should be developed with high specific surface area and large proportion of meso-pores.

In such situation, two dimensional (2D) materials have great potential towards adsorption processes due to its high surface to volume ratio unlike, its bulk
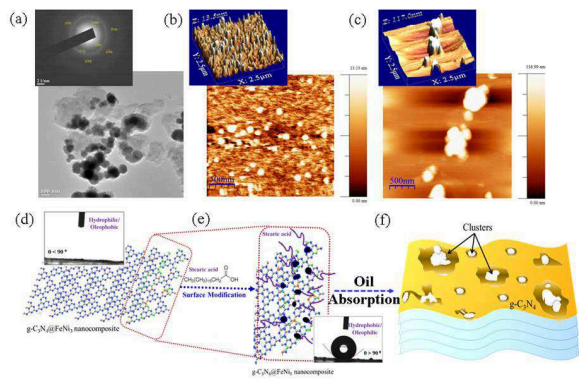
* Corresponding Author: pdeb@tezu.ernet.in

FIG. 2. (a)TEM micrograph of surface modified g-C_3N_4@$FeNi_3$ nanocomposite before oil absorbtion with SAED pattern embedded at the left top, AFM 2D images of the surface modified nanocomposite (b) before oil absortion and (c) after oil absorption embeded with their respective 3D image on the left top. (d) hydrophilic/oleophobic surface of nanocomposite showing contact angle below 90^0 and (e) surface modified to hydrophobic/oleophilic showing contact angle above 90^0. (f) The final surface topography of the material is shown after oil absorption corroborating AFM image.
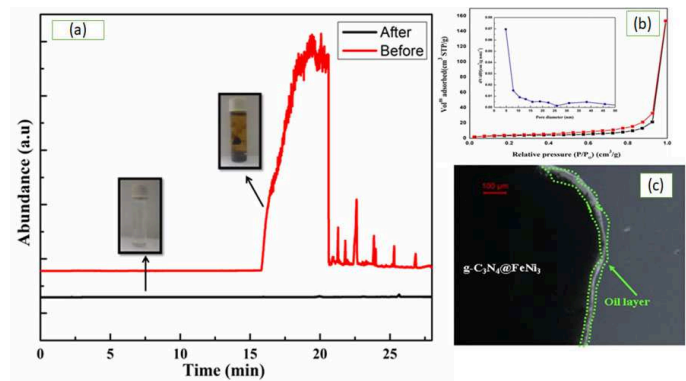

FIG. 3. (a) GC-MS plot of the surface modified composite before and after oil absorptions. (b) Nitrogen adsorption-desorption isotherm, where the pore size distribution of the same is in the inset. (c) Light microscope image showing the oil presence on the surface of the composite.

form [14]. Besides, for decent adsorption outcome, high content of carbon and nitrogen are preferred to present as a prerequisite in the adsorbent moiety. The strategy here is to employ graphitic C_3N_4, which provides high surface area owing to its 2D sheet structure. Nontoxic iron nickel ($FeNi_3$) magnetic nanoparticles (MNPs) have been mixed with graphitic carbon nitride (g-C_3N_4) to form the composite material (shown in toc Fig. 1). The layers in the g-C_3N_4 sheet are connected via tertiary amines in a stacked fashion and separated by weak van der Waals (vdW) forces. The vdW force hardly regulate the uniform delocalization (i.e. the distribution of magnetic spheres) of $FeNi_3$ MNPs on the sheet surface enhancing the sorption capability of the host flakes. Besides, the nanocomposite exhibits hydrophobic and oleophilic properties after surface engineering with stearic acid ($CH_3(CH_2)_{16}COOH$), which makes the oil extraction easy and effective. Moreover, the nanocomposite efficiently removes variety of oils from water surface under an external magnet.

The minimum energy based structures of the composite system are fixed using geometry optimization via Broyden-Fletcher-Goldfarb-Shanno (BFGS) algorithm [15]. The geometry optimization is fixed via affecting the organizing atoms in the supercell to minimum total energy position for stable geometry (Figure 1) with its electronic structure to verify its stability.

A representative TEM image of the composite system before surface modification was shown in Figure2 (a)

with its SAED pattern and schematic structure with contact angle (Figure 2 (d)). The image revealed uniformity in shape and size of MNPs, with a diameter around 70 nm over the sheet surface in the composite system. A stacked graphitic structure was noticed with the dispersion of MNPs on the carbon nitride sheets impeding the formation of composite system. SAED pattern indicated that the nanoparticles are polycrystalline in nature with (002), (111) and (100) planes of both FeNi_3 and g-C_3N_4 identified in the composite. AFM images of the system were shown in Figure2 (b) and (c)) to visualize the surface topography before and after oil removal, respectively along with their schematic structure (Figure 2 (e) and (f)) for easy visualization. AFM images provided convincing evidence regarding post-oil absorption enhancement in MNP size indicating the formation of finite number of nanoparticle clusters over the sheet surface. Also, the images revealed the uniform increase of nine times in thickness of the nanosheets after oil absorption (Figure 2 (c)) compared to the pristine nanosheets (Figure 2(b)).

Micro-structural study of the composite was carried out through x-ray diffraction (Figure S2-4). The diffraction peaks observed at 2=27.40, 44.10, 51.30 and 75.70 in the composite system indexed to (002), (111), (200) and (220) lattice planes respectively. The above results endorsed the formation of g-C_3N_4@$FeNi_3$ composite. However, the peak intensity became weaker and the width of the diffraction peak became broader indicating interactions between MNPs and host sheet due to presence of Fe in the composite system.

We first used a laser with 514 nm wavelength with hardly detectable Raman peaks. Fluorescence background of the composite suppressed the Raman peaks at lower wavelength excitation source of 514 nm [16]. Lastly, 699 cm^{-1} was due to bending and stretching

mode on ring atoms of NCN and CN (shown in Table S1). Due to breaking of the cyano group, no further Raman modes were obtained beyond 1650 cm-1 (Figure S6). With rise in temperature from 450^0 C to 550^0 C, the crystalline phase transforms to complete amorphous state corroborating our XRD results [17].

The GC-MS characterization (Figure 3(a)) was performed to confirm the adsorption of the viscous oil and its removal efficacy. It was observed that several chromatographic peaks were present revealing the existence of crude oil in the oil-water mixture before oil removal. The water, left-over in the Petri dish after oil adsorption, was tested again and found no such peaks. The absence of aforementioned peaks indicated the absence of oil in the oil water mixture showing efficient oil removal by the composite.

The FTIR spectra of g-C_3N_4 sheet were plotted for 450^0 C and 550^0 C and 500^0 C for comparison with the composite system. The adsorption band of composite system at 1605 cm^{-1} were assigned to C=N. Similarly, the absorption bands at 1257, 1311 and 1424 cm^{-1} were assigned to aromatic C-N stretching heterocycles. The presence of MNPs suppressed the peak intensity in case of composite suggesting weak interaction between the other carbon and nitrogen bonds [18]. The textural properties of carbon nitride based catalysts were studied by nitrogen sorption. Figure 3(b) displayed the absorption-desorption isotherm curves of g-C_3N_4 sheet showing a characteristic of type IV isotherm pattern. The surface area was found to be 41 m^2g^1 for g-C_3N_4 from the Brunauer-Emmett-Teller (BET) curve. Barrett-Joyner-Halenda (BJH) curve indicated the pore-size distribution of the flake reflecting the existence of mesopore in the flake structure (inset of Figure 3(b)). The pore-size distribution curve showed the mesoporous structure with the pore size in the range of 4-40 nm. The textural property of the g-$C_3N_4@FeNi_3$ is basically consistent with that of g-C_3N_4 support, suggesting that the FeNi3 nanoparticles do not block the pore distribution on the sheet surface. Figure 3(c) gives the light microscopic image of the oil absorbed g-C3N4@FeNi3 surface. The spotted green colour dotted line reveals the presence of crude oil on nanocomposite surface.

The surface engineering enabled in wettability transition of the nanocomposite, which was ensured by contact angle measurements before and after oil absorption (shown inset of Figure 4a (i) and (ii) respectively). The increase in contact angle upto 140 implied the hydrophobic and oleophilic nature of the prepared nanocomposite material. The shape of the water droplet above the sample was uniform and indicating the surface to be highly hydrophobic. The contact angle showed hydrophobic behavior after reusing the composite for oil removal for the second time (shown inset of Figure 4a (ii)). The nanocomposite retained its hydrophobic
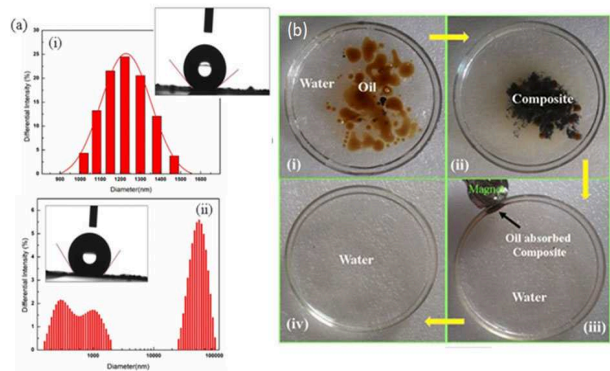

FIG. 4. Particle size distribution pattern of (a) surface modified g-$C_3N_4@FeNi_3$ nanocomposite (i) before oil absorbtion embe dded (right hand top position of the image) with contact angle and (ii) after oil absorption inset with contact angle showing hydrophobic and oleophilic behaviour. (b) Removal process of crude oil ((i)-(iv)) from water surface by nanocomposite under magnetic eld.

and oleophilic behavior after its first use which showed the transition in wettability nature due to good stearic acid based surface engineering of the nanocomposite. The dynamic light scattering (DLS) measurements are shown in Figure 4a (i) and (ii), which evaluated the hydrodynamic diameters. The hydrodynamic diameter was obtained to be almost 1.2 μm before oil extraction, while this diameter value increased significantly after oil adsorption. The hydrodynamic diameter, measured by DLS, was affected by the viscosity and concentration of the medium. As a result, the value was larger than that the value obtained from TEM image of the same system (Figure 2a).

The highly hydrophobic and oleophilic nanocomposite exhibited a selective absorbance for oil recovery. When brought into contact with a layer of crude oil in oil-water mixture, the nanocomposite adsorbed the oil instantaneously repelling the water. Interestingly, the oil-adsorbed nanocomposite could be removed from oil-water mixture with an external magnet with a very quick response. The process of oil absorption and removal is shown in Figure 4b (i) to (iv) in stepwise manner.

The outcome efficacy is measured using the formula [19]

$$n = (m_2 - m_1)/c_0$$

where m_1 is the weight of nanocomposite before extraction and m_2 is the weight of nanocomposite after oil extraction. c_0 is the weight of the added crude oil. The outcome efficiency of crude oil extraction is found to be 92 % with the prepared magnetic nanocomposite. Apart from crude oil separation, other oils such as Mobil,
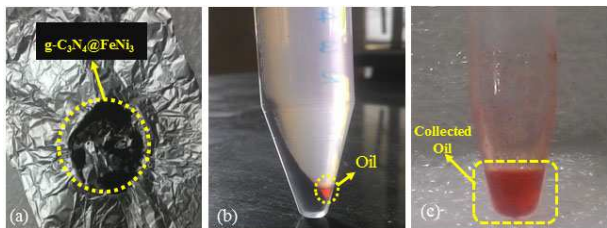
FIG. 5. The collected surface modified g-$C_3N_4@FeNi_3$ nanocomposite (a) is washed (b) and oil is collected (c).

Petrol and Mustard oil were also used in extraction process. It has been found that surface modified 2D g-$C_3N_4@FeNi_3$ can also be used to separate these variety of oils. Apart from crude oil separation, it showed noted removal efficiency in case of other oils.

The nanocomposite can be further recycled and reused for oil adsorption and separation in an ecofriendly manner as shown in Figure 5. The graphitic magnetic nanocomposite once used can be recycled and reuse again. The system can be further reused easily by washing the composite with ethanol and then drying at a temperature of 60^0 C. The removed oil can be recovered successfully, apart from its reusability. Figure 5(c) shows the recovery of oil after separation.

In summary, we develop a novel and smart surface engineered sorbent material to realize magnetic separation of oil from oily water mixtures. The stearic acid based surface functionalized porous graphitic flakes exhibit not only wettability transition from hydrophilicity to hydrophobicity, but also selective oleophilicity in oil removal from water body. 2D graphitic flatland with precise surface area and high proportion of mesopore achieves near-absolute adsorption efficiency of crude oil. As a result, the sheet thickness enhanced upto 9 folds compared to the pristine one. The developed system efficiently recovers crude oil from water surface under an external magnet with a quick response. Apart from the crude oil, the composite system selectively adsorbs a wide range of oils. Moreover, we present density functional theory DFT calculations to validate the stability and sorption activity of the composite system. Thus, the prepared g-$C_3N_4@FeNi_3$ nanocomposite acts as promising absorbent material for efficient oil recovery and hence provides feasible solution towards the upcoming oil consumption.

[1] W. X. Z. B. H. . W. J. H. L. Lee, Q. Kalb, Science **328**, 76 (2010).

[2] A. Jernelov, Nature **466**, 182 (2010).

[3] A. A. Keller and V. Broje, Environ. Sci. Technol. **40**, 7914 (2006).

[4] H. M. Choi and R. M. Cloud, Environ. Sci. Technol. **26**, 772 (1992).

[5] D. L. V. A. K. B. K. L. M. C. R. E. B. Kujawinski, M. C. K. Soule, Environ. Sci. Technol. **45**, 1298 (2011).

[6] M. H. I. L. M. S. M. H. A. Aziz, M. A. Zahed, Bioresour. Technol. **101**, 9455 (2010).

[7] S. P. S. R. K. T. I. Buist, J. McCourt, Pure Appl. Chem. **71**, 43 (1999).

[8] . L. V. A. K. B. . . L. M. C. R. E. B. Kujawinski, M. C. K. Soule, Environ. Sci. Technol. **45**, 1298 (2011).

[9] K. H. A. Vidyasagar and K. M. Sureshan, Angew. Chem. Int. Ed. **50**, 8021 (2011).

[10] V. Broje and A. A. Keller, Environ. Sci. Technol. **40**, 7914 (2006).

[11] X. W. J. Z. L. J. D. L. Tian, X. F. Zhang, Phys. Chem. Chem. Phys. **13**, 14606 (2011).

[12] C. G. H. Sun, Z. Xu, Adv. Mater. **25**, 2554 (2013).

[13] X. T. J. G. B. D. Y. Si, J. Yu, Nat. Commun. **5**, 5802 (2014).

[14] N. N. P. d. V. P. R. C. M. E. G.-T. S. E. S. A. C. M. E. S. S. Barg, F. M. Perez, Nat. Commun. **5**, 4328 (2014).

[15] D. L. S. Q. Y. C. W. Lei, D. Portehault, Nat. Commun. **4**, 1777 (2013).

[16] X. W. K. T. D. J. H. D. E. P. A. D. Liao, J. Z. Wu, Phys. Rev. Lett. **106**, 256801 (2011).

[17] T. L. T. . . J. . K. C. . L. S. .-H. C. J. . M. T. Rojalin, L. Kurki, Anal. Bioanal. Chem. **408**, 761 (2016).

[18] R. D. Z. X. S. D. R. L. Z. L. J. Z. X. Gao, J. Zhou, Adv. Mater. **28**, 168 (2016).

[19] C. Y. Z. D. L. J. C. Li, L. Wu, Angew. Chem. **129**, 3811 (2017).